Dynamical bunching and density peaks in expanding Coulomb clouds

X. Xiang,[*] B. Zerbe,[†] Others TBA, and P. M. Duxbury[‡]
Department of Physics and Astronomy, Michigan State University
(Dated: June 13, 2017)

We show that the expansion dynamics of charged particle clouds, such as electron pulses used in ultrafast electron microscopy, show novel behavior due to high acceleration of particles in the cloud interior. This often leads to electron bunching and dynamical formation of a density peak in the outer regions of the bunch. We develop analytic fluid models to capture these effects, and the analytic predictions are validated by PIC and N-particle simulations. When starting from rest, two and three dimensional systems with Gaussian initial densities show bunching and a strong peak response, while one dimensional systems do not; moreover these effects can be tuned using the initial particle density profile and velocity chirp.

High charge density systems arise in a variety of physical contexts ranging from astrophysics[need references]; accelerator technology [need references]; electron microscopy[need references, Jensen, Rose, Jensen etc.]; to high power vacuum electronics[need references, Zheng etc.]. Understanding of the dynamics of spreading of such systems is critical to the design of next generation technologies, and simple analytic models are particularly helpful for instrument design. As a result, substantial theoretical efforts have already been made in this vein[Jensen,Reed,Siwick,the accelerator theory papers]. Specifically, free expansion of clouds of charged particles starting from rest have been well studied both analytically and computationally [Grech and the like], and a number of studies have found evidence of the formation of a region of high-density on the periphery of the clouds under certain conditions[Grech,Russian papers,Reed].

One application of these theories that is of particular current interest is to high density electron clouds used in ultrafast electron microscopy (UEM). In the UEM community, researches have conducted substantial theoretical treatment of initially extremely short bunches of thousands to hundreds of millions of electrons that operate in a regime dominated by a virtual cathode (VC) limit which is independent from the Child-Langmuir current limit[Valfells, Qian, Siwick, Reed, Collins, others]. These photo-emitted electron bunches typically have an in-plane, "transverse" extent that is typically of order one hundred microns, while the longitudinal spread is typically of order fifty femtoseconds, which corresponds to sub-micron widths[King2005 and modern reviews]. After photoemission, the electrons are extracted longitudinally using either a DC or AC field typically in the hundreds of kV[our work, Miller's work, Luiten's work] or low MV [Musucemi] ranges, respectively. However, the theoretical treatments of such "pancake-like" electron bunch evolution have largely focused on the longitudinal dimension, and the few studies looking at transverse dynamics have either assumed a uniform-transverse distribution [1] or have looked at the effect of a smooth Gaussian-to-uniform evolution of the transverse profile on the evolution of the pulse in the longitudinal direction[2]. Of specific note, only one analytic study found any indication, a weak longitudinal signal, of forementioned high-density peripheral regions[2].

On the other hand, an attractive theoretical observation relevant to a number of fields is that an ellipsoidal cloud of cool, uniformly distributed charged particles has a linear electric field within the ellipsoid which results in maintenance of the uniform charge density as the cloud spreads [Grech and others?]. In the UEM community, such a uniform distribution is a prerequisite in employing techniques such as emittance compensation [reference]. To create such uniform charge distributions, it has long been proposed that the formation of a uniform ellipsoid may be generated through proper control of the transverse profile of a short charged-particle bunch emitted from a source into vacuum[3], and experimental results have shown that an electron cloud emitted from a photocathode and accelerated into the highly-relativistic regime has a shadow that is characteristics of such a uniform distribution[4]. Contrary to expectations from the free expansion work but consistent with the longitudinal analyses, this shadow lacks any indication of a peripheral region of high-density as expected from free-expansion studies. However, recent work has indicated that a substantial high density region may indeed form in the transverse direction[Ruan's transverse], and N-particle simulation results, as demonstrated in Fig. (1), demonstrate a substantial ring-like region of high density circumscribing the median of the bunch.

Here we demonstrate the formation of a ring-like high-density region within both N-particle and particle in cell (PIC) simulations of electron bunches with initial transverse Gaussian profile and offer an explanation on why this phenomena has not been noted previously within the
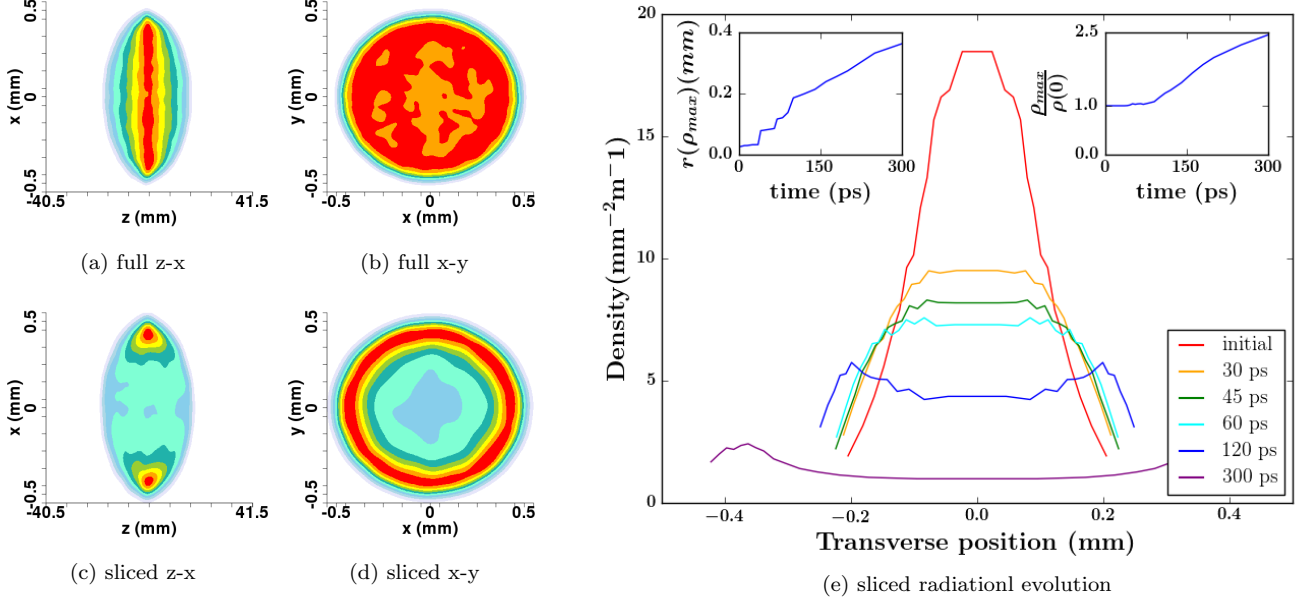
(a) full z-x   (b) full x-y

(c) sliced z-x   (d) sliced x-y

(e) sliced radiationl evolution

FIG. 1. (a-d.) Two dimensional projections of 1×10^6 electron positions simulated with the N-particle code, COSY, for approximately 300 ps after injection with a Gaussian ($\sigma_r = 100~\mu m$) transverse profile into a cavity with an electric field of 10 MV/m. Colors are from white to red representing linear ranges. Other simulations (not shown) have confirmed the presence of the ring-like density after nanoseconds. (a.) and (b.) are projections of the full distribution to the x-z and x-y planes, respectively. (c.) and (d.) are x-z and x-y projections, respectively, of just the portion of the distribution within 20% of the standard deviation of the median value of y and z, respectively. Notice the ring-like substructure that is evident in the "slices", (c.) and (d.) but is absent from the full distribution projections, (a.) and (b.). (e.) N-particle radial-distribution obtained near the longitudinal median plane of the bunch at various times. Density is calculated by binning 1000 macroparticles and assigning the resulting density to the average radial position. The initial distribution is approximately Gaussian, and the square-like nature of the plot results from the discreteness of the bins. The sub-graph in the upper left corner shows the position of max density as a function of time, which is non-zero at initial time due to binning resulting in a non-zero minimum radial position. The sub-graph in the upper right shows the ratio of the max density to the density at the minimum r value. Notice, the "phase transition" in the 45-80 ps range where the location of the non-zero, non-stochastic peak first appears well away from the origin.

UEM literature. We then utilize a Poisson fluid approach to derive analytic predictions for the dynamics of high charge density particle systems under one-dimensional, cylindrical, and spherical geometries that should be relevant to a large number of physical communities, and we derive conditions for the emergence of density peaks distinct from any initial density maximum. We show that peak formation has a strong dependence on dimension, with one dimensional systems having strict conditions on parameters for bunching whereas higher dimensional systems have strict conditions on parameters to prevent bunching. Additional PIC and N-particle simulations are used to validate the analytical predictions for peak emergence derived from the analytical charged-particle dynamics.

One reason that this phenomenon has not been seen previously is apparent in Fig. (1). Previous studies, including our own work, have looked at the projection of the distribution to the x-z plane[references]. Fig. (1) shows that by projecting the distribution in this manner with the ability to only discern density fluctuations at about the 10% level results in the density substructure primarily along the bunch median is lost; however, by restricting the projection to only electrons near the median of the bunch, a restriction that can only be done computationally presently, results in evidence of a transverse ring-like density substructure near the median longitudinal position. Therefore, the full density projection obscures this signal suggesting possible substructure information is lost by this analytic strategy at typical density-detection resolutions.

A second reason that this phenomenon has not been seen previously is apparent in Fig. (2) which presents a qualitative description of when to expect the emergence of the ring-like substructure. Specifically, most analytic work has been conducted using $\leq$ 10k electrons with a transverse standard deviation of 100 μm, and this structure is not apparent for at least 500 ps. Moreover, even when using the slicing analytic strategy, this structure is barely discernible from stochastic noise. Also, as can be seen in Fig. (2), the pulse emergence time is essentailly a constant factor times the plasma period. We derive the
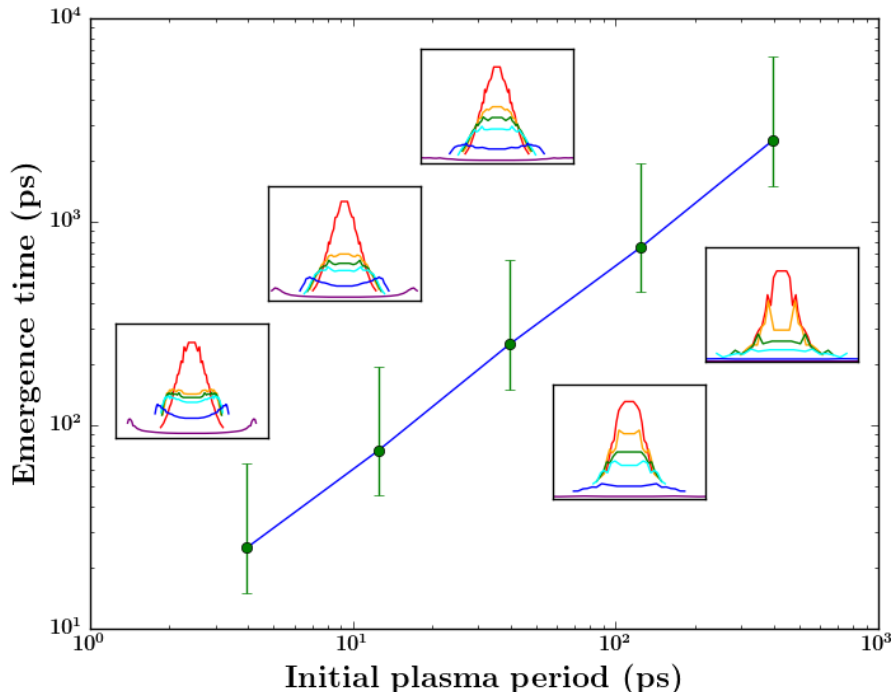
FIG. 2. Qualitative observation of emergence of the ring-like density pulse as a function of initial plasma period, $\tau_p = \sqrt{\frac{m\epsilon_0}{q^2 n}}$, with n representing the number density, of the bunch as predicted by N-particle simulations. Sub-graphs show the normalized-density evolution within 5x the initial transverse standard deviation of the bunch taken at time points of roughly 0 (red), 2.5 (yellow), 3.75 (green), 5 (blue), 10 (cyan), and 25 (purple) times the plasma period and are directly above or below their corresponding point. Normalized density are calculated by binning a number of macroparticles and assigning the resulting density to the average radial position as was also done in Fig (1e). The initial distribution is Gaussian, and the square-like nature of the sub-plots results from the discreteness of the bins. Notice that the density pulse is more prominent in the higher-dose distributions but is evident in all simulations emerging somewhere in the $2.5\tau_p$ to $10\tau_p$ range indicated on the main plot by error bars despite the presence of more stochastic effects in the lower doses. Low dosage (corresponding to the three larger plasma period times) plots fail to capture the full width of the bunch at 25 τ_p due to spreading beyond ± 0.5 m resulting from the initial velocity spread and the long density pulse emergence time; however, we have kept the scale to demonstrate the main features of the density pulse evolution. Due to the large error bars of the density pulse emergence time resulting from the qualitative nature of the observation, we do not provide the equation of the line here.

corresponding factor explicitly for cylindrical and spherical symmetries later in this manuscript.

Due to the appearance of this ring-like phenomenon in both N-particle and PIC simulations, we conclude that applying a mean-field like reasoning applied to the transverse expansion of the bunch should be able to capture the gross dynamics. Distilling this reasoning, a distribution that is originally more dense toward the center, then particles toward the center should experience more radial force resulting in an inverse velocity chirp that results in ring-like build-up of electrons. However, it is not immediately apparent why such dynamics are almost entirely absent in the longitudinal direction as found by numerous studies [references]; therefore, we develop a theory to describe this understanding in one, two, and three dimensions where analytic progress is possible due to the unique properties of the Coulomb interaction in special

symmetric geometries.

Consider the non-relativistic spreading of a electron bunch in a one dimensional model, which is a good approximation to the longitudinal spreading of a pancake-shaped electron cloud generated at a photocathode. In one dimensional models, the charge density only depends on one co-ordinate, which we take to be the $z-axis$. For the sake of readability, denote $z = z(t)$ and $z_0 = z(0)$ and denote the charge distribution at all times to be $Q_{\text{tot}}\rho(z,t)$ with $\rho(z,t)$ a unitless, probability-like density and Q_{tot} the total charge in the bunch. Further, abbreviate $\rho(z_0,0)$ as ρ_0. In one dimensional models, the amount of distribution to either side of the particle determines the field at the particle resulting in a monotonic electric field, and in the absence of any particle crossover, this field, and hence the resulting particle acceleration, $a(z,t)$ is independent of time providing $a(z,t) = a(z_0,0)$

abbreviated as a_0 and thus suggesting that the details of the density evolution are captured by the relation between z and z_0. However, due to the constant nature of a_0, this relation is the elementary constant acceleration kinematic equation

$$z = z_0 + v_0 t + \frac{1}{2} a_0 t^2 \tag{1}$$

where v_0 is the initial velocity of the charged particle at z_0. In general, both v_0 and a_0 are functions of the initial position, z_0, and the special case of $v_0 = 0$ everywhere, which we will call the cold-case, is commonly assumed in the literature [references]. Notice, that particle crossover should never occur in the cold case resulting in this description being valid for 1D cold case dynamics for all time.

Since particles may neither be created nor destroyed in our model, we have

$$\rho(z,t)dz = \rho_0 dz_0 \tag{2}$$

so that in the non-relativistic case derived above,

$$\rho(z,t) \frac{= \rho_0 \left(\frac{dz}{dz_0}\right)^{-1} = \rho_0}{1 + v_0' t + \frac{1}{2} a_0' t^2} \tag{3}$$

where $v_0' = \frac{dv_0}{dz_0}$ and $a_0' = \frac{da_0}{dz_0}$. Consider a freely expanding initial charge distribution that is symmetric and initially centered at $z = 0$ in the non-relativistic limit. The charge distribution evolves under the influence of the internal space charge forces leading to

$$a_0 = \frac{qQ_{\text{tot}}}{2m\epsilon_0} \delta\sigma, \tag{4}$$

where q is the charge of the particle, m is its mass, and

$$\delta\sigma = \int_{-z_0}^{z_0} \rho_0(z) dz, \tag{5}$$

Notice via the Fundamental Theorem of Calculus that the derivative of the acceleration with respect to the initial position is directly proportional to the initial distribution

$$a_0' = \frac{qQ_{\text{tot}}}{2m\epsilon_0} \frac{d\delta\sigma}{dz_0}$$
$$= \frac{qQ_{\text{tot}}}{m\epsilon_0} \rho_0 \tag{6}$$

where the symmetric nature of ρ_0 was used to eliminate the factor of 2. Plugging Eq. (6) into Eq. (3), we get

$$\rho(z,t) = \frac{\rho_0}{1 + v_0' t + \frac{qQ_{\text{tot}}}{2m\epsilon_0}\rho_0 t^2} \tag{7}$$

$$\frac{d}{dz}\rho(z,t) = \frac{\rho_0'(1 + v_0' t) - \rho_0 v_0'' t}{\left(1 + v_0' t + \frac{qQ_{\text{tot}}}{2m\epsilon_0}\rho_0 t^2\right)^3} \tag{8}$$

where $\rho_0' = \frac{d\rho_0}{dz_0}$ and $v_0'' = \frac{d^2 v_0}{dz_0^2}$. A detailed derivation of the second expression is done in the Supplemental. For the cold-case, Eq. (7) reduces to density evolution derived by Reed[2]. Also, in the cold-case, Eq. (8) simplifies into a proportionality between the initial slope of the distribution and the slope of the distribution at any later time. Therefore, a charge distribution that is initially at rest and unimodal, i.e only a single initial location has non-zero density with $\rho_0' = 0$, never develops a dynamically generated second maximum. This explains why we should not expect to see a density ridge in the longitudinal direction while the 1D model is applicable in the cold-pancake regime. The extension of this description to asymmetric functions is straightforward, as is the inclusion of an image field at the photocathode. However, inclusion of these effects does not change Eq. (7), Eq. (8), nor the conclusions we have drawn from them. The non-cold case will be discussed elsewhere.

The constant acceleration approximation and absence of particle crossovers is not valid in the cylindrical and spherical geometries, nevertheless analytic results are still possible prior to particle crossover in the non-relativistic regime. Consider a non-relativistic evolving distribution $Q_{\text{tot}}\rho(r,t)$, where $\rho(r,t)$ is again taken to be the unitless particle distribution and Q_{tot} is again the total charge in the bunch. In a system with cylindrical symmetry, the mean field equation of motion for a charge at $r \equiv r(t)$ is given by,

$$\frac{d\vec{p}_{\text{2D}}}{dt} = \frac{qQ_{\text{tot}}\lambda(r,t)}{2\pi\epsilon_0 r}\hat{r} \tag{9}$$

where $\lambda(r,t)$ is the linear charge inside radius r calculated by $\lambda(r,t) = \int_0^r 2\pi\tilde{r}\rho(\tilde{r},t)d\tilde{r}$ again normalized so that $\lambda(r,t) \leq 1$. Analogously in a system with spherical symmetry, the equation of motion for an electron at position r is given by

$$\frac{d\vec{p}_{\text{3D}}}{dt} = \frac{qQ_{\text{tot}}Q(r,t)}{4\pi\epsilon_0 r^2}\hat{r} \tag{10}$$

where $Q(r,t) = \int_0^r 4\pi\tilde{r}^2\rho(\tilde{r},t)d\tilde{r}$ again normalized so $Q(r,t) \leq 1$. Notice, r in Eq. (9) denotes the cylindrical radius while r in Eq. (10) represents the spherical radius , and the ambiguity will be maintained throughout the text. In both situations, before any crossover occurs, the charge integrals are constant. That is, we may write $\lambda(r,t) = \lambda(r_0,0) \equiv \lambda_0$ and $Q(r,t) = Q(r_0,0) \equiv Q_0$ for a particle starting at $r_0 \equiv r(0)$. $Q_{\text{tot}}\lambda_0$ and $Q_{\text{tot}}Q_0$ can be interpreted as the charged contained in the appropriate Gaussian surface, and if we track the particle that starts at r_0, these contained charges should remain constant before any crossover occurs. It is convenient to also define the average particle density to be $\bar{\rho}_0 = \frac{\lambda_0}{\pi r_0^2}$ in the 2D case and $\bar{\rho}_0 = \frac{Q_0}{\frac{4\pi r_0^3}{3}}$ in the 3D case. Notice that this average particle densities are a function solely of r_0, and

we will use later in the text. Eq. (9) and Eq. (10) may now be rewritten as

$$\frac{dp_{r,2D}}{dt} = \frac{qQ_{tot}\lambda_0}{2\pi\epsilon_0 r} \tag{11}$$

$$\frac{dp_{r,3D}}{dt} = \frac{qQ_{tot}Q_0}{4\pi\epsilon_0 r^2} \tag{12}$$

for the period of time before particle crossover and where all time dependence in the force is accounted for by the r term in the denominator.

Since Eq. (11) and Eq. (12) represents the force on the particle in the cylindrical and spherical contexts, respectively, we can integrate over the particle's trajectory to calculate the change in the particle's energy. Integrating from $r_0, 0$ to r, t gives

$$E_{2D}(r,t) - E(r_0,0) = \frac{qQ_{tot}\lambda_0}{2\pi\epsilon_0} ln\left(\frac{r}{r_0}\right) \tag{13}$$

$$E_{3D}(r,t) - E(r_0,0) = \frac{qQ_{tot}Q_0}{4\pi\epsilon_0}\left(\frac{1}{r_0} - \frac{1}{r}\right) \tag{14}$$

where the term on the right side of the equality can be interpreted as the change in the potential energy within the self-field of the bunch.

These expressions are fully relativistic, and in the non-relativistic limit, we can derive the position-time relation for the particle. The details of this derivation have been placed in the on-line Supplement, and the resulting expressions in the cold-case are presented here

$$t_{2D} = \frac{\bar{\tau}_{p,0}}{\pi}\frac{r}{r_0}F\left(\sqrt{ln\left(\frac{r}{r_0}\right)}\right) \tag{15}$$

$$t_{3D} = \sqrt{\frac{3}{2}}\frac{\bar{\tau}_{p,0}}{2\pi}\left(\tanh^{-1}\left(\sqrt{1-\frac{r_0}{r}}\right) + \frac{r}{r_0}\sqrt{1-\frac{r_0}{r}}\right) \tag{16}$$

where $F(\cdot)$ represents the Dawson function and $\bar{\tau}_{p,0}$ represents the plasma period determined from the initial conditions by $\bar{\tau}_{p,0} = 2\pi\sqrt{\frac{m\epsilon_0}{qQ_{tot}\bar{\rho}_0}}$ indicating that the appropriate time scale is essentially the plasma period as determined qualitatively in Fig. (2). Furthermore, the time-position relation detailed in these equations depends solely on the amount of charge nearer to the origin than the point in question, i.e. $Q_{tot}\bar{\rho}_0$, consistent with Gauss's law and not on the details of the distribution. Notice, however, that each initial position can have a different time constant, and that it is the relationship between the time-position relationships of different locations where the details of the distribution become important and may cause neighboring particles to have interesting relative dynamics.

To understand these dynamics we generalize Eq. (3),

$$\rho(r,t) = \rho_0\left(\left(\frac{r}{r_0}\right)^{d-1}\frac{dr}{dr_0}_d\right)^{-1} \tag{17}$$

where d is the dimensionality of the problem, i.e. 1, 2 or 3 in this text. The factor in the denominator, $\frac{dr}{dr_0}_d$, may be determined implicitly from the time-position relations above, as we've done this in general in the Supplement We again present the expressions in the cold case for $d = 2$ and $d = 3$

$$\frac{dr}{dr_0}_d = \frac{r}{r_0}\left(1 + \frac{d}{2}\left(\frac{\rho_0}{\bar{\rho}_0} - 1\right)f_d\left(\frac{r}{r_0}\right)\right) \tag{18}$$

where $f_2\left(\frac{r}{r_0}\right) = 2\sqrt{\ln\left(\frac{r}{r_0}\right)}F\left(\sqrt{\ln\left(\frac{r}{r_0}\right)}\right)$ and $f_3\left(\frac{r}{r_0}\right) = \frac{r_0}{r}\sqrt{1-\frac{r_0}{r}}\tanh^{-1}(\sqrt{1-\frac{r_0}{r}}) + 1 - \frac{r_0}{r}$. For further analysis, call $D_d = D_d(r_0) = \frac{d}{2}\left(\frac{\rho_0}{\bar{\rho}_0} - 1\right)$ the divergence from uniform function in 2 and 3 dimensions. These D functions are solely functions of the initial conditions and are positive at locations where the local density is larger than the average density, negative when the density is smaller than the average density, and identically zero when the average density is identical to the local density. Specifically, for a uniform distribution with an infinitely sharp cutoff in either the cylindrical or spherical case, the corresponding D function is zero at every location where the original density is defined. Thus, the uniform density evolution in Eq. (17) reduces to the generally recognized [citations] $\rho(r,t)\pi r^2 = \rho_0\pi r_0^2$ in the cylindrical case and $\rho(r,t)\frac{4}{3}\pi r^3 = \rho_0\frac{4}{3}\pi r_0^3$ in the spherical case. However, Eq. (18) is general for any distribution before particle crossover, not just the uniform distribution.

Again, analogous to the one dimensional case, particle crossover occurs when $\frac{dr}{dr_0}_d = 0$. For a particle starting at position r_0 and having a divergence from uniform function $D_d(r_0)$, crossover occurs when the particle is at a position, r, that satisfies $f_{dD}(r,r_0) = -1/D_d(r_0)$. Since every particle expands in this model, every particle will have a time for which it will assume every value of the function $f(r,r_0)$. The character of the two and three dimensional f's are similar as can be seen in Fig (3) where the value of the function is plotted against $\frac{r_0}{r}$. Specifically, both functions increase to a maximum and then asymptote towards 1 from above. This means that all density positions eventually experience uniform-like scaling since $\lim_{r\to\infty} f_{dD}(r,r_0) = 1$ results in Eq. (17) simplifying to $\rho\pi r^2 = \rho_0\frac{\pi r_0^2}{1+D_{dD}(r_0)}$ and $\rho\frac{4}{3}\pi r^3 = \rho_0\frac{\frac{4}{3}\pi r_0^3}{1+D_{dD}(r_0)}$ in the cylindrical and spherical cases, respectively, for large enough r. The main differences are that the cylindrical function's max is larger than the spherical function's, $max(f_{2D}) \approx 1.28$ vs $max(f_{3D}) \approx 1.07$, and occurs at a larger value of $\frac{r_0}{r}$ than the spherical function, $r \approx 9.54r_0$ instead of $r \approx 8.27r_0$, respectively. The first observation means cylindrical symmetry is more sensitive to the distribution than spherical symmetry, whereas the second means that if crossover is going to occur for a specific particle, it will occur before the r value for
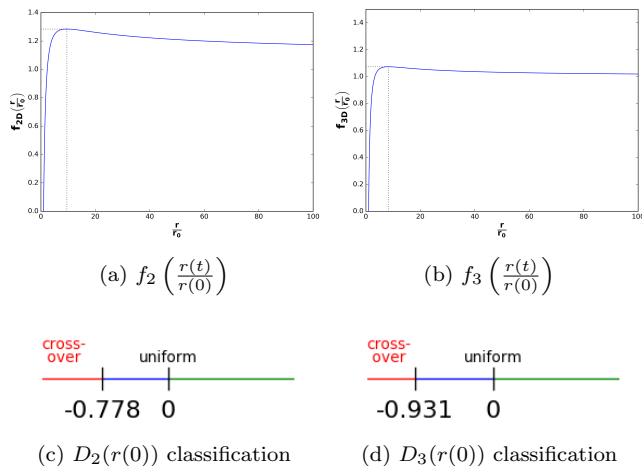
(a) $f_2\left(\frac{r(t)}{r(0)}\right)$

(b) $f_3\left(\frac{r(t)}{r(0)}\right)$

(c) $D_2(r(0))$ classification

(d) $D_3(r(0))$ classification

FIG. 3. (a-b.) Plot of the $f_{2\mathrm{D}}$ and $f_{3\mathrm{D}}$ functions against $\frac{r}{r_0}$. Since particles are always expanding in our model, $\frac{r}{r_0} \geq 1$ and goes to infinity for infinite time. Notice that both functions have similar character with a maximum in the $8-10\ r_0$ range eventually approach 1 from above. Dashed lines indicate the location of the functions' maximum. These functions allow us to classify the distribution by the initial value of $D_{\mathrm{dD}}(r_0) = \frac{d}{2}\left(\frac{\rho_0(r_0)}{\bar{\rho}_0(r_0)} - 1\right)$ as is done in (c-d.). Specifically, regions experiencing crossover (local contraction), in red, the uniform distribution, when $D_{\mathrm{dD}}(r_0) = 0$, and regions experiencing more or less expansion than the uniform distribution, in green and blue, respectively are marked in the figures.

which the corresponding f function is maximum (i.e. $r \approx 9.54 r_0$ or $r \approx 8.27 r_0$), otherwise the particle will never experience crossover. However, too much should not be made of this observation as once crossover has occurred farther from the center of the distribution than a given point, this given point may eventually crossover the crossed over point as the crossed over point no longer can be described by our model. Nevertheless, we may obtain the earliest time of crossover before which our model is completely valid as a mean-field theory. This can be obtained by minimizing the time with the crossover constraint $\frac{dr}{dr_0}\Big|_{\mathrm{d}} = 0$ by such methods as Lagrange multiplies, where the Lagrangian has the following form

$$\mathcal{L}_{\mathrm{dD}} = t_{\mathrm{dD}} - \lambda\left(1 - \frac{d}{2}\left(\frac{\rho_0(r_0)}{\bar{\rho}_0(r_0)} - 1\right)f_{\mathrm{dD}}(r, r_0)\right) \quad (19)$$

To demonstrate the use of these equations, we present the evolution of the initially-at-rest cylindrically- and spherically- symmetric uniform distribution of 1.875×10^7 and 2^4 electrons within radii's of 1 mm (see Fig. (4(a,b)). Note, in this fairly trivial case, crossover should not occur and the analytic results should be valid mean-field-results for all time. As can be seen in Fig. (4(a,b)), the evolution of the uniform distribution in both PIC and N-particle simulations is captured by the analytic solution. Specifically, the distributions simply expand while remaining uniform, and the analytic formulation correctly calculate the rate of this expansion.

Less trivially is the evolution of Gaussian distributions. We simulated 3.75×10^7 and 10^5 electrons for the cylindrical and spherical cases, respectively, using $\sigma_r = 1$ mm. Solving for the minimum crossover time, we get approximately and 44 ns for each distribution. Therefore, we simulate for 37.5 ns, which is well before any crossover events. As can be seen in Fig. (4), both the cylindrically- and spherically- symmetric Gaussian distributions develop peaks similar to what is seen in our disc-like simulations, and this "phase-like" transition arise on the order of approximately 20 ps. Also, as can be seen in Fig. (4), both the PIC and the N-particle results match the analytical results extremely well. The primary differences between the cylindrically- and spherically- symmetric evolutions is in their rate of width expansion and in the sharpness of the peak that forms, both of which are captured by the analytic models. In addition, the analysis presented here may be carried out utilizing $\rho_0(\phi, r, z) = \sigma_0(\phi, r)\delta(z - z_0)$ to model the UEM pancake regime expansion, but this results in a slightly different interpretation of the D function than the spherical case presented above and these details will be presented elsewhere.

CONCLUSIONS

0. Summary of findings. 1. Steady state Child-Langmuir current should not have this a. Non-steady state bunches though... depends on profile and initial density b. This possibly has wide applicability 2. Bi-modal distributions and rms emittance a. Explains Luiten's observations b. Can be ameliorated at the cost of loss of electrons 3. A deeper study of this phenomena is warranted 4. We have not really discussed emittance, and further study on emittance is warranted. In particular the dynamical formation of a density peak near the edges of the bunch, in the transverse direction, leads to opportunities to improve the brightness and coherence length critical to ultrafast electron microscopy and may be exploited in other fields.

† zerbe@msu.edu
‡ duxbury@msu.edu

[1] S. Collin, M. Merano, M. Gatri, S. Sonderegger, P. Renucci, J.-D. Ganiere, and B. Deveaud, Journal of applied physics **98**, 094910 (2005).

(a) cylindrical symmetry uniform

(b) spherical symmetry uniform

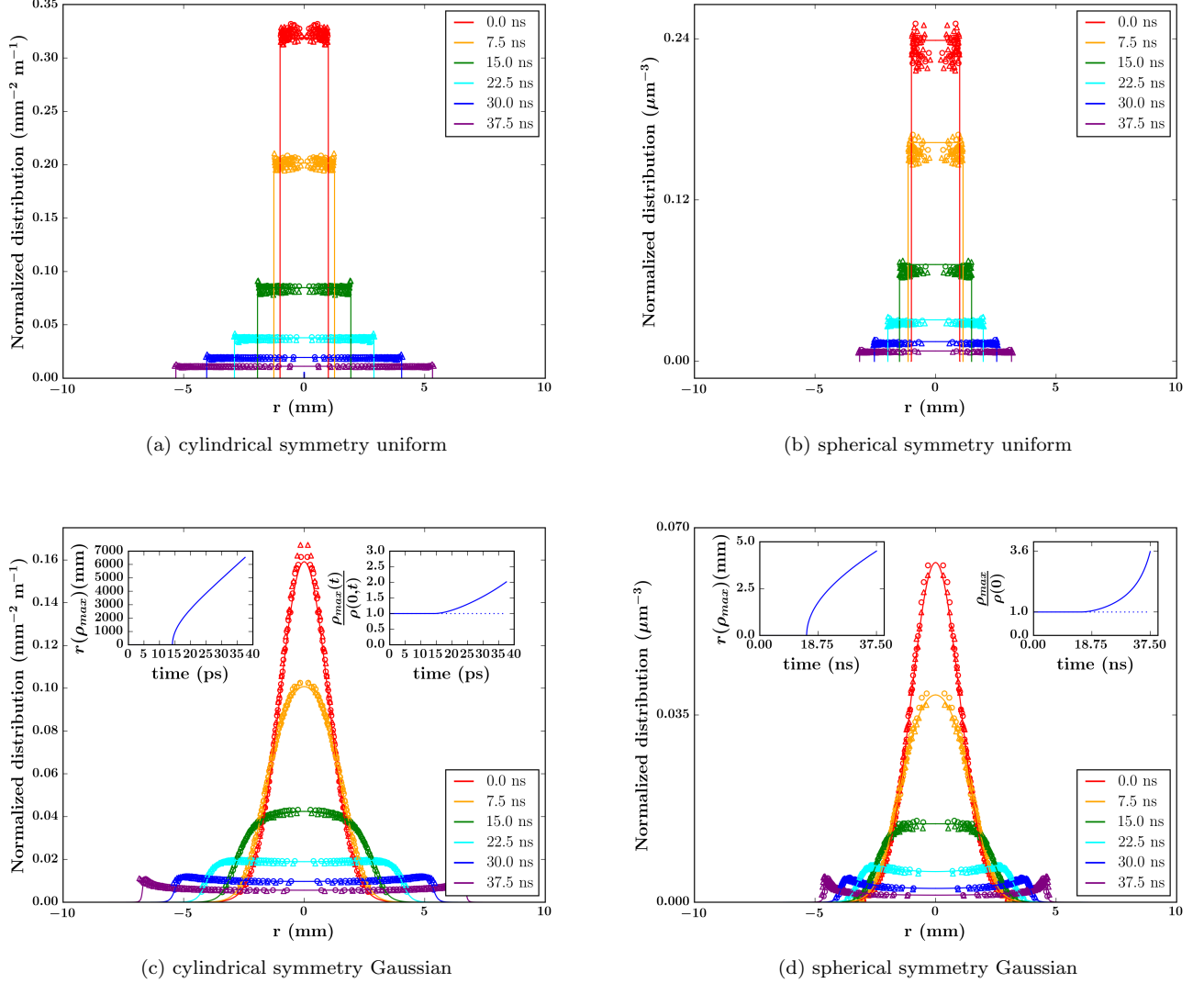(c) cylindrical symmetry Gaussian

(d) spherical symmetry Gaussian

FIG. 4. Analytical (solid line), PIC (cirlces), and N-particle (triangles) results of the normalized density evolution of (a.,c.) cylindrically and (b., d.) spherically symmetric (a., b.) uniform and (c.,d.) Gaussian distributions with $R = \sigma_r = 1$ mm and N of 1.875×10^7, 2×10^4, 3.75×10^7, and 10^5 electrons, respectively, before any analytic crossover events. The sub-graph in the upper left corner of (c.,d.) shows the analytic position of max density as a function of time, and the sub-graph in the upper right of (c.d.) shows the analytic ratio of the max density to the density at the minimum r value both. The corresponding analytic ratio for the uniform distribution is shown in this sub-graph as a dashed horizontal line at 1. Unsurprisingly, the PIC results and the analytical results, both mean-field models, are in almost perfect agreement, and the N-particle results are in surprisingly good agreement as well. Notice that the models predict peak formation on a time-scale dependent on the initial plasma frequency similar to the peak formation seen in the N-particle disc-like density evolution seen in Fig. (1(e.)) and detailed in Fig. (2).

[2] B. W. Reed, Journal of Applied Physics **100**, 034916 (2006).

[3] O. J. Luiten, S. B. V. D. Geer, M. J. D. Loos, F. B. Kiewiet, and M. J. V. D. Wiel, Physical review letters **93**, 094802 (2004).

[4] P. Muscemi, J. T. Moody, R. J. England, J. B. Rosenzweig, and T. Tran, Physical review letters **100**, 244801 (2008).